Postprint. Hao Qin et al., Journal of Molecular Liquids, Volume 326 (2021) 115292
https://doi.org/10.1016/j.molliq.2021.115292

Physical Absorption of Carbon Dioxide in Imidazole-PTSA based Deep Eutectic Solvents

Hao Qin[a], Zhen Song[b], Hongye Cheng[a,*], Liyuan Deng[c], Zhiwen Qi[a,*]

[a]*State Key Laboratory of Chemical Engineering, School of Chemical Engineering, East China University of Science and Technology, 130 Meilong Road, Shanghai 200237, China*

[b]*Process Systems Engineering, Otto-von-Guericke University Magdeburg, Universitätsplatz 2, D-39106 Magdeburg, Germany*

[c]*Department of Chemical Engineering, Norwegian University of Science and Technology, Sem Sælandsvei 4, 7491 Trondheim, Norway*

[*]*Corresponding author:* hycheng@ecust.edu.cn (Cheng)*;* zwqi@ecust.edu.cn (Qi)

Abstract

Capture of CO_2 with high efficiency is essential to tackle the global warming issue that has aroused widespread attention. Herein we employed the halogen-free deep eutectic solvents (DESs) consisting of imidazole (Im) and *p*-toluenesulfonic acid (PTSA) to absorb CO_2. The CO_2 solubility in [3Im:PTSA], [3.5Im:PTSA], and [4Im:PTSA] is measured in the range of temperature from 303.15 to 333.15 K and pressure from 110 to 1500 kPa. Henry's constants of H_x and H_m and thermodynamic properties of $\Delta_{sol}G$, $\Delta_{sol}H$, and $\Delta_{sol}S$ are correlated from the experimental data. The comparison between the studied DESs and the reported solvents is performed based on H_m. Afterwards, the experiment-dependent Jou and Mather empirical model and fully predictive COSMO-RS model are used to calculate the CO_2 solubility, which are compared with the experimental results. Finally, the interaction energies between CO_2 and DESs, as indicated by misfit, hydrogen bond, and van der Waals energies, are calculated by COSMO-RS to illustrate the absorption mechanism.

Keywords: Halogen-free deep eutectic solvent; CO_2 solubility; solubility fitting;

COSMO-RS evaluation; interaction analysis

1. Introduction

In the past decades, global warming has aroused increasing concerns over the world. The massive emission of CO_2, mainly derived from fossil fuel power plants, is being considered the mainspring [1-3]. Therefore, CO_2 capture and storage have been of central importance to reduce CO_2 concentration. The most prevalent technology is post-combustion capture based on the chemical absorption employing aqueous solutions of alkanolamines [4-7]. However, this process suffers from several drawbacks, such as severe equipment corrosion, high solvent loss, and large operation costs [8-11]. From the green chemistry and sustainability point of view, it is greatly advisable to develop environmentally friendly and highly efficient alternatives to the traditional alkanolamines.

Ionic liquids (ILs), namely liquid salts, have been extensively studied as promising candidates to absorb CO_2 in the last few years [12-14]. This category of ionic compounds consists of asymmetric cations and anions, owning a broad liquid range including room temperature. Besides, the high thermal and chemical stability, as well as negligible vapor pressure, enable them to serve as a potential replacement of the conventional absorbents [15-19]. Nevertheless, the complex preparation, high cost, and toxicity of ILs cause economic and environmental challenges for both the industry and academia. Therefore, deep eutectic solvents (DESs) have been currently thrust into the limelight as IL analogues, which refer to the mixtures of Lewis or Brønsted acids and bases to present much lower freezing points than the individuals [20-22]. While keeping the favorable properties of ILs, DESs exhibit unique superiority such as simple preparation, low price, flexible designability, and reasonable biodegradability, which render them as “advanced ILs” [23-26].

The fascinating properties of DESs have triggered considerable attention across various chemical processes like bio-refining [27], chemical reaction [28], liquid-liquid extraction [20] and gas absorption [29], among which CO_2 absorption is particularly attractive. Li et al. investigated the CO_2 absorption using DESs at moderate pressures

and temperature ranging from 303.15 to 343.15 K, where DESs are formed by choline chloride (ChCl) as hydrogen bond acceptor (HBA) and glycerol and ethylene glycol as hydrogen bond donors (HBDs) [30,31]. Deng et al. reported the CO_2 solubility in the eutectic mixtures formed by ChCl and various HBDs, i.e., phenol, dihydric alcohols, furfuryl alcohol, and levulinic acid [32-34]. In our recent work, four phosphonium-based DESs were prepared to absorb CO_2 under 313.15-333.15 K and pressure below 2000 kPa, and molecular dynamics (MD) simulations were performed to gain a deep insight into the microscopic behaviors of DESs and {DES + CO_2} mixtures [35]. However, despite the progress, the researches using DESs to capture CO_2 are still relatively scarce that mostly focus on the ChCl-based ones. Actually, large amounts of potential combinations of HBA and HBD are regarded as promising CO_2 absorbents. Moreover, considering the green chemistry concept, the involvement of halogens may be not environmentally friendly [36,37].

In our previous work, we developed the acid-base tunable DESs prepared by imidazole (Im) and *p*-toluenesulfonic acid (PTSA) [38]. In this contribution, due to the Lewis acidity of CO_2, we tune the mole ratio of Im to PTSA into the weak basic region to obtain the room temperature and halogen-free basic DESs of [3Im:PTSA] (DES1), [3.5Im:PTSA] (DES2), and [4Im:PTSA] (DES3). The CO_2 solubility in these halogen-free DESs are experimentally determined, and important thermodynamic properties are correlated. The experimental data are then compared with those (1) predicted by Conductor-like Screening Model for Real Solvents (COSMO-RS) and (2) calculated by Jou and Mather empirical model. Finally, the absorption mechanism is investigated by the interaction energy analysis using the COSMO-RS.

2. Method Description

2.1 Chemicals

The cylinder of CO_2 was purchased from Shanghai Wetry Standard Reference Gas Co., Ltd. (Shanghai, China) with purity of 99.999%. Imidazole (Im) and *p*-

toluenesulfonic acid (PTSA) were supplied by Adamas-beta (Shanghai, China) with purity above 99%. All the chemicals were used as received without further purification.

2.2 DES preparation

The specific amounts of Im and PTSA in different mole ratios (3:1, 3.5:1, and 4:1) were weighted using the Sartorius BSA224S-CW balance with the precision of ± 0.0001 g. Afterward, the mixtures were heated and magnetically stirred at 353.15 K and 800 rpm to obtain homogenous liquids. The temperature was controlled within a fluctuation of ± 0.1 K (Huber Ministat 230, Germany). The molecular weight of DES is defined as,

$$M_{DES} = \sum_i x_i M_i \tag{1}$$

where x_i and M_i are the mole fraction and molecular weight of the DES species i (cation, anion, or HBD), respectively. The density of DESs was measured by a digital density meter (Anton Par, DMA-4500 M, Austria). The viscosity of DESs was determined using a rheometer (Anton Par, MCR302, Austria) with the shearing rate of 100 s^{-1}.

2.3 Determination of CO_2 solubility

The CO_2 solubility in DESs was measured using the pressure drop method, under the pressure and temperature varying from 110 to 1500 kPa and 303.15 to 333.15 K, respectively. The experimental setup and procedures have been elaborately described in our earlier work [8,35,39]. The mole fraction (x_{CO_2}) and molality (m_{CO_2}) of CO_2 in DESs can be calculated as follows,

$$x_{CO_2} = n_{CO_2}/(n_{CO_2} + n_{DES}) \tag{2}$$

$$m_{CO_2} = n_{CO_2}/w_{DES} \tag{3}$$

where n_{CO_2} denotes the mole quantity of CO_2 in DESs; n_{DES} and w_{DES} are the mole quantity and mass of DESs, respectively.

2.4 Uncertainty calculation

For an input quantity X_i derived from n independent repeated observations $X_{i,k}$, the input estimate x_i is usually determined as the sample mean,

$$x_i = \overline{X_i} = \frac{1}{n}\sum_{k=1}^{n} X_{i,k} \tag{4}$$

The standard uncertainty $u(x_i)$ of its estimate x_i can be defined as the experimental standard deviation [40,41],

$$u(x_i) = s(\overline{X_i}) = \sqrt{\frac{1}{n(n-1)}\sum_{k=1}^{n}(X_{i,k} - \overline{X_i})^2} \tag{5}$$

The calculated standard uncertainties of $u(x)$ and $u(m)$ for the mole fraction and molality of CO_2 in DESs are less than 0.0006 and 0.0018 mol·kg^{-1}, respectively.

2.5 COSMO-RS calculation

The COSMO-RS, a predictive model that is fully independent of experimental data, proves to be efficient in predicting and interpreting the thermodynamic properties of fluid phases [42-44]. In this work, the COSMO-RS calculations were performed with the BP_TZVP_C30_1401 parametrization in COSMOthemX (Version C30_1401). The COSMO files of CO_2 and imidazole were directly taken from the database, while the COSMO files of DES species of Im^+ and PTS^- were obtained through the geometry optimization using the Gaussian 03 package with the BP86/TZVP basis set.

According to the COSMO-RS theory, the gas solubility can be calculated in an iterative procedure; that is, the mole fraction x_j is varied until the partial pressure p_j equals to the given reference pressure p. The p_j is determined by equation (6),

$$p_j = p_j^0 x_j \gamma_j \tag{6}$$

where γ_j stands for the activity coefficient, and p_j^0 represents the vapor pressure of pure compound. Here p_j^0 is estimated using the COSMOtherm approximation of the vapor pressure using the exact gas phase energy of the compound from the .energy file [45]. The activity coefficient in system S can be predicted as follows,

$$\gamma_S^X = \exp[(\mu_S^X - \mu_X^X)/kT \quad (7)$$

The gas phase is assumed ideally. γ_j is computed by varying x_j in each step of the iteration, then p_j is calculated according to the equation (6).

Moreover, relying on the statistical thermodynamic principles, the software can compute the molecular energy of the electrostatic misfit, hydrogen bond (HB), and van der Waals (vdW) interactions, which are three important energy descriptors in COSMO-RS theory. The calculation details are shown in equation (8)-(10) [46,47],

$$E_{misfit}(\sigma, \sigma') = a_{eff}\frac{\alpha'}{2}(\sigma + \sigma') \quad (8)$$

$$E_{HB} = a_{eff}c_{HB}\min[(0; \min(0; \sigma_{donor} + \sigma_{HB}))\ \max(0; \sigma_{acceptor} - \sigma_{HB})] \quad (9)$$

$$E_{vdW} = a_{eff}(\tau_{vdW} + \tau'_{vdW}) \quad (10)$$

where five parameters are referred including the interaction parameter (α'), the effective contact area (a_{eff}), the hydrogen bond strength (c_{HB}), the threshold for hydrogen bonding (σ_{HB}), and the element-specific vdW interaction parameter (τ_{vdW}).

3. Results and Discussion

3.1 CO_2 solubility in the DESs

The densities and viscosities of DESs are firstly measured at the temperature range of 303.15-333.15 K. From Figure 1(a), the density shows a negative linear correlation with the temperature, which can be described as:

$$\rho = a + bT \quad (11)$$

The parameters a and b can be fitted. The Vogel−Fulcher−Tamman (VFT) model is used to describe the viscosities of DESs:

$$\eta = \exp(\mathrm{A} + \mathrm{B}/(\mathrm{T} - T_0)) \quad (12)$$

where A, B, and T_0 are empirical constants. The DESs present a good fluidity with viscosity lower than 60 mPa·s. Afterward, as tabulated in Table 1, the solubility of CO_2 in the three DESs are determined as a temperature and pressure dependent function,

expressed as mole fraction (x_{CO_2}) and molality (m_{CO_2}), respectively.

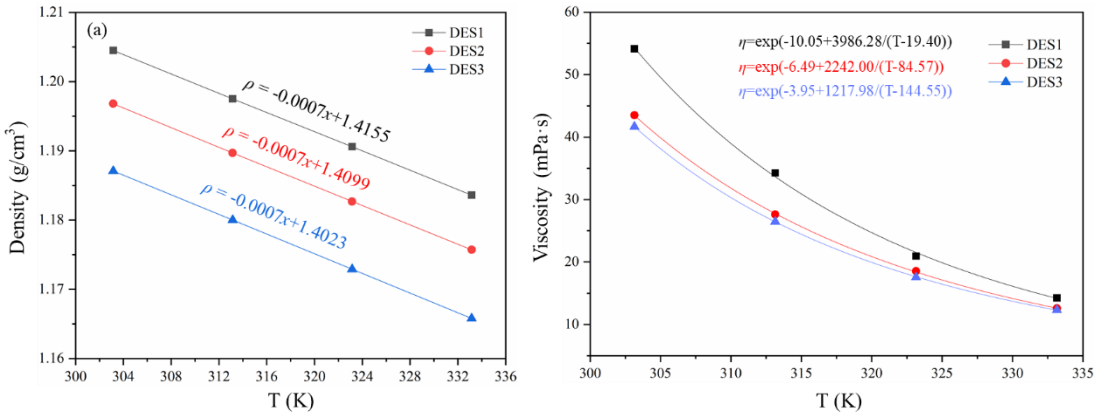

Figure 1. (a) Density and (b) viscosity of DESs as a function of temperature.

The pressure dependence of the CO_2 solubility is illustrated in Figures 2 and 3. As seen, it grows linearly with the increasing pressure and decreasing temperature, and the extrapolation line almost passes through the coordinate origin, suggesting the physical absorption behavior of CO_2 in the DESs. Moreover, the CO_2 solubility in the DESs increases slightly varying from DES1 to DES3.

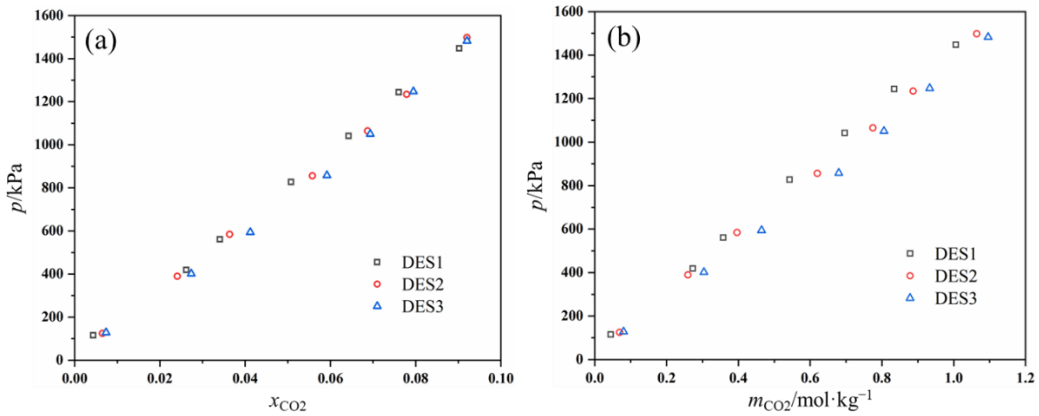

Figure 2. CO_2 solubility in halogen-free DESs at 303.15 K (a) mole fraction (b) molality.

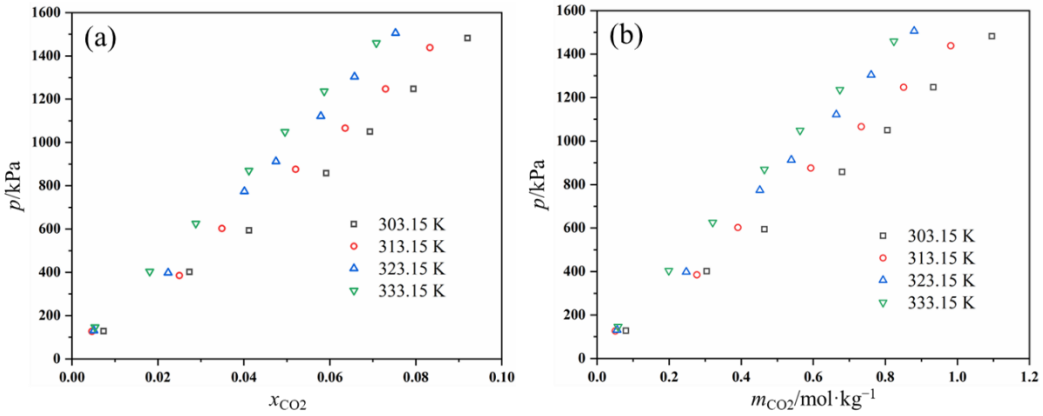

Figure 3. CO_2 solubility in DES3 at different temperatures (a) mole fraction (b) molality.

Postprint. Hao Qin et al., Journal of Molecular Liquids, Volume 326 (2021) 115292
https://doi.org/10.1016/j.molliq.2021.115292

Table 1. CO_2 solubility in the DESs as a function of temperature and pressure.[a]

T=303.15K			*T*=313.15K			*T*=323.15K			*T*=333.15K		
p/kPa	m_{CO2} /mol·kg^{-1}	x_{CO2}	*p*/kPa	m_{CO2} /mol·kg^{-1}	x_{CO2}	*p*/kPa	m_{CO2} /mol·kg^{-1}	x_{CO2}	*p*/kPa	m_{CO2} /mol·kg^{-1}	x_{CO2}
DES1											
115.7	0.0446	0.0044	119.1	0.0406	0.0040	144.0	0.0558	0.0055	144.5	0.0387	0.0038
418.6	0.2728	0.0262	347.9	0.1820	0.0176	428.0	0.2233	0.0215	433.0	0.1967	0.0190
561.0	0.3580	0.0341	559.6	0.3253	0.0311	621.7	0.3429	0.0327	621.3	0.2924	0.0280
827.6	0.5425	0.0508	812.0	0.5044	0.0474	846.3	0.4801	0.0452	918.0	0.4598	0.0434
1041.5	0.6966	0.0643	1041.7	0.6452	0.0598	1052.0	0.5886	0.0549	1097.8	0.5491	0.0514
1243.7	0.8346	0.0760	1253.2	0.7853	0.0719	1245.5	0.7099	0.0654	1250.2	0.6297	0.0587
1447.5	1.0059	0.0902	1443.3	0.9001	0.0815	1441.2	0.8028	0.0734	1420.0	0.7354	0.0676
DES2											
124.5	0.0691	0.0065	133.6	0.0546	0.0052	138	0.0541	0.0051	150.9	0.0486	0.0046
389.2	0.2595	0.0241	389.3	0.2212	0.0206	398.8	0.2127	0.0199	400.9	0.1971	0.0184
584	0.3965	0.0364	624.1	0.4321	0.0395	599.4	0.3392	0.0313	594.8	0.2947	0.0273
855.7	0.6202	0.0558	984.9	0.6694	0.0599	882.1	0.5188	0.0471	885.3	0.4707	0.0429
1064.6	0.7751	0.0687	1150.3	0.7731	0.0686	1077.5	0.6175	0.0555	1070.4	0.5678	0.0513
1234.5	0.8872	0.0779	1301.2	0.8516	0.0750	1261.2	0.7429	0.0661	1260.6	0.6638	0.0595
1498.2	1.0642	0.0920	1567.5	0.9950	0.0865	1426.4	0.8269	0.0744	1502.9	0.7894	0.0699
DES3											
128.2	0.0801	0.0074	126.9	0.0508	0.0047	131.2	0.0555	0.0051	146.1	0.0581	0.0053
401.8	0.3040	0.0274	384.8	0.2771	0.0250	398	0.2473	0.0224	404	0.1990	0.0181
594.2	0.4646	0.0412	602.2	0.3910	0.0349	774	0.4518	0.0401	625.7	0.3207	0.0288
857.8	0.6800	0.0592	875.8	0.5932	0.0520	912.8	0.5388	0.0475	869.7	0.4643	0.0412
1050.3	0.8057	0.0694	1066.1	0.7337	0.0636	1121.6	0.6642	0.0579	1048.9	0.5634	0.0495
1247.1	0.9333	0.0795	1247.4	0.8507	0.0730	1303.6	0.7606	0.0657	1236.3	0.6739	0.0587
1482.1	1.0959	0.0920	1438.5	0.9819	0.0833	1505.6	0.8802	0.0753	1459.3	0.8238	0.0708

[a] Standard uncertainties u are $u(T)$ = 0.1 K, $u(p)$ = 0.2 kPa, $u(x)$ = 0.0006, $u(m)$ = 0.0018 mol·kg^{-1}

3.2 Henry's constant

The physical absorption behavior follows the Henry's law, and the mole fraction-based Henry's constant can be defined as:

$$H_x(T,P) = \lim_{x_{CO_2}\to 0} \frac{f^L_{CO_2}(T,P)}{x_{CO_2}} = \lim_{x_{CO_2}\to 0} \frac{P\phi_{CO_2}(T,P)}{x_{CO_2}} = \frac{P_e}{x_{CO_2}} \quad (13)$$

where $f^L_{CO_2}$ is the fugacity of CO_2, ϕ_{CO_2} is the fugacity coefficient, and P_e is the system pressure at equilibrium. At the range of moderate pressure studied in this work, $f^L_{CO_2}$ is assumed to be equal to P_e.

Similar to $H_x(T,P)$, the molality-based Henry's constant can be deduced as:

$$H_m(T,P) = \lim_{m_{CO_2}\to 0} \frac{f^L_{CO_2}(T,P)}{m_{CO_2}} = \lim_{m_{CO_2}\to 0} \frac{P\phi_{CO_2}(T,P)}{m_{CO_2}} = \frac{P_e}{m_{CO_2}} \quad (14)$$

where m_{CO_2} is the molality of CO_2 in the DESs.

The constants of H_x and H_m can be obtained by linearly fitting pressure with mole fraction and molality of CO_2, respectively, which are presented in Table 2. As a smaller value of Henry's constant reflects a higher absorption capacity, Henry's constant increases with the temperature, indicating a lower absorption capacity at a higher temperature [39,48,49]. The DES3 [4Im:PTSA] possesses smaller Henry's constants (H_m =1.3324-1.8525 MPa·kg·mol^{-1}) than those of DES2 [3.5Im:PTSA] (H_m =1.3995-1.9065 MPa·kg·mol^{-1}) and DES1 [3Im:PTSA] (H_m =1.4814-1.9854 MPa·kg·mol^{-1}). Therefore, the CO_2 capture capacity in the DESs is ranked as [4Im:PTSA] > [3.5Im:PTSA] > [3Im:PTSA].

Table 2. Henry's constants of CO_2 in DESs at different temperatures.

DESs	H_m/MPa·kg·mol^{-1}				H_x/MPa			
	303.15K	313.15K	323.15K	333.15K	303.15K	313.15K	323.15K	333.15K
DES1	1.4814	1.6152	1.7846	1.9854	16.208	17.567	19.259	21.301
DES2	1.3995	1.5267	1.7249	1.9065	15.889	17.272	19.167	21.231

DES3	1.3224	1.4674	1.7037	1.8525	15.450	17.208	19.624	21.009

3.3 Comparison of absorption capacity

The molality-based H_m provides a uniform scale to evaluate the absorption capacity of different solvents. The comparison between the studied DESs and the reported solvents at 313.15 K are summarized in Table 3. The studied DESs show a lower level of H_m than many other HBA:HBD combinations, which still holds when compared to the cases of commercial PEGs, FAPE-1215 and ionic liquids [hhemel], [hmim][BF_4]. However, the CO_2 solubility in present DESs is lower than that of commercial PC and NHD. In addition, although the DESs of ChCl:urea (1:2.5 and 1:2) and ChCl:ethylenecyanohydrin (1:2 and 1:3) exhibit a higher absorption capacity, the studied DESs also demonstrate its superiority taking the halogen-free advantage into account. To sum up, the satisfactory CO_2 absorption capacity of DESs [4Im:PTSA], [3.5Im:PTSA], and [3Im:PTSA] are confirmed.

Postprint. Hao Qin et al., Journal of Molecular Liquids, Volume 326 (2021) 115292
https://doi.org/10.1016/j.molliq.2021.115292

Table 3. Comparison of H_m in the studied DESs with that in previously reported solvents at 313.15 K.

Absorbents	H_m/MPa·kg·mol^{-1}	References
Im:PTSA (3:1)	1.62	This work
Im:PTSA (3.5:1)	1.53	This work
Im:PTSA (4:1)	1.47	This work
ACC-Tri (1:1)	3.15	[48]
ACC-Im (2:3)	3.09	[48]
ACC-Im (1:2)	2.82	[48]
ACC-Im (1:3)	2.32	[48]
ChCl:guaiacol (1:5)	3.84	[56]
DH:guaiacol (1:5)	3.01	[56]
ACC:guaiacol (1:5)	3.54	[56]
ChCl:urea (1:2.5)	1.37	[50]
ChCl:urea (1:2)	1.29	[50]
ChCl:glycerol (1:2)	1.70	[31]
ChCl:ethylene glycol (1:2)	2.71	[30]
ChCl:lactic acid (1:2)	4.00	[57]
ChCl:levulinic acid (1:3)	2.62	[33]
ChCl:ethylenecyanohydrin (1:2)	0.99	[49]
ChCl:ethylenecyanohydrin (1:3)	1.09	[49]
PEG150	2.25	[39]
PEG200	2.11	[39]
PEG300	1.98	[39]
PEG400	1.91	[39]
PC	0.72	[58]
FAPE-1215	1.70	[59]
NHD	1.05	[60]
[hhemel]	5.38	[61]
[hmim][BF4]	1.81	[62]

Postprint. Hao Qin et al., Journal of Molecular Liquids, Volume 326 (2021) 115292
https://doi.org/10.1016/j.molliq.2021.115292

3.4 Thermodynamic properties

The thermodynamic properties are correlated from Henry's constant using the following equations:

$$\Delta_{sol}G = RTln(H(T,P))/P^0 \quad (15)$$

$$\Delta_{sol}H = R\left(\frac{\partial \ln(H(T,P)/P^0}{\partial(1/T)}\right) \quad (16)$$

$$\Delta_{sol}S = (\Delta_{sol}H - \Delta_{sol}G)/T \quad (17)$$

where $\Delta_{sol}G$, $\Delta_{sol}H$ and $\Delta_{sol}S$ are the solution Gibbs free energy, solution enthalpy, and solution entropy, respectively; P^0 is the standard pressure of 0.1 MPa.

Table 4. Calculated thermodynamic properties at 0.1 MPa and 303.15 K

DESs	$\Delta_{sol}G$/kJ·mol^{-1}	$\Delta_{sol}H$/kJ·mol^{-1}	$\Delta_{sol}S$/J·mol^{-1}·K^{-1}
DES1	12.82	-7.64	-67.49
DES2	12.77	-8.16	-69.04
DES3	12.70	-8.86	-71.12

As shown in Table 4, the positive value of $\Delta_{sol}G$ signifies that the absorption process is nonspontaneous behavior. The negative $\Delta_{sol}H$ indicates that the CO_2 dissolution in the DESs is exothermic. In comparison with other absorbents (e.g. -11.18 kJ·mol^{-1} in PEG400 [39], -17 kJ·mol^{-1} in [ChCl:2urea] [50], and -17.24 kJ·mol^{-1} in [bmim][PF_6] [51]), the smaller absolute values of $\Delta_{sol}H$ suggest lower regeneration energy consumption and process cost for the studied DESs [35,48,52]. Moreover, the negative $\Delta_{sol}S$ means a higher-order degree after CO_2 absorption.

3.5 Solubility fitting and COSMO-RS evaluation

The experiment-dependent Jou and Mather empirical model [53,54] is used to fit the CO_2 solubility data with partial pressure and temperature, which is given in equations (18)-(20):

$$lnp = A + Bln\alpha \quad (18)$$

$$A = a + bT + cT^2 \quad (19)$$

$$B = e + fT + gT^2 \quad (20)$$

where p is the partial pressure of CO_2, α is the CO_2 loading in the liquid phase in mol CO_2/mol DES; T is the temperature in K; A and B are the functions of temperature. The coefficients are correlated and listed in Table 5, and the calculated and experimental x_{CO_2} are compared and illustrated in Figure 4a. Moreover, the COSMO-RS model is employed to calculate the CO_2 solubility at the specific temperature and pressure to evaluate its prediction performance, as described in the aforementioned method (Section 2.5). The comparison between the calculated and experimental x_{CO_2} is depicted in Figure 4b.

Table 5. The correlation coefficients of Jou and Mather empirical model.

DESs	a	b/K^{-1}	c/K^{-2}	d	e/K^{-1}	f/K^{-2}
DES1	-11.737	0.0692	-9.725×10^{-5}	-17.028	0.1130	-1.788×10^{-4}
DES2	11.508	-0.0776	1.333×10^{-4}	23.875	-0.1415	2.170×10^{-4}
DES3	1.250	-0.0158	4.125×10^{-5}	24.147	-0.1454	2.268×10^{-4}

The model deviation is indicated as average relative deviation (ARD) according to the equation (21),

$$ARD(\%) = \frac{1}{n}\sum_{n}\left|\frac{x_{CO_2,exp} - x_{CO_2,cal}}{x_{CO_2,exp}}\right| \times 100 \quad (21)$$

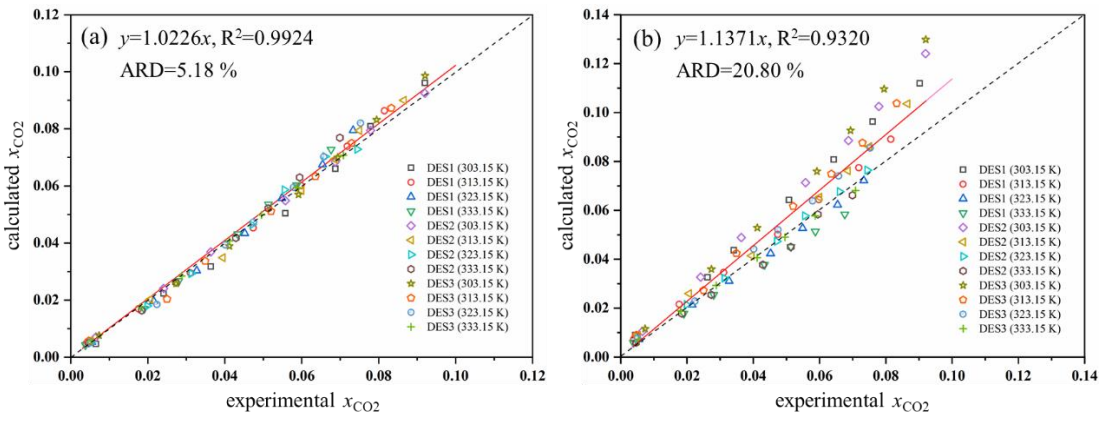

Figure 4. Comparison between calculated and experimental CO_2 solubility. (a) Jou

and Mather empirical model; (b) COSMO-RS model. Dotted line: $y = x$; solid line: linear fit.

From Figure 4a, the experimental results agree well with that calculated by Jou and Mather empirical model, with a small ARD of only 5.18 %. In comparison from Figure 4b, despite some reasonable deviations (ARD = 20.80 %), the COSMO-RS predicted results are in good agreement with the experiments, as suggested by the high value of R^2 (0.9320). Moreover, considering the fully predictive character of COSMO-RS, the predictions are quite acceptable [55].

3.6 Analysis of absorption mechanism

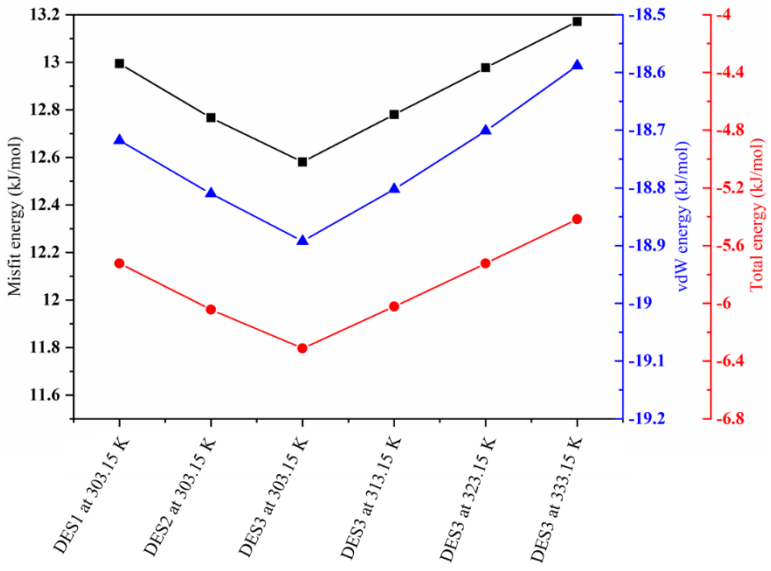

Figure 5. COSMO-RS interaction energies between CO_2 and DESs

To demonstrate the absorption mechanism, the misfit, HB, and vdW interaction energies between CO_2 and DESs are calculated by COSMO-RS. The positive and negative energy reflects the repulsive and attractive interaction between CO_2 and DES, respectively. The HB interaction between CO_2 and DESs is not observed, due to the nonpolar nature of CO_2. As shown in Figure 5, from DES1 to DES3 at 303.15 K (the left three data points), the positive misfit energy decreases with the increasing Im content in DESs, suggesting that the repulsive electrostatic effect is weakened. On the contrary, the negative value of vdW energy identifies the attractive effect of DES towards CO_2, and the absolute vdW energy value increases with the Im content. With

the decreasing repulsive interaction (misfit) and increasing attractive interaction (vdW), DES3 exhibits a more negative total energy with CO_2 than DES 2 and DES1, which is in accordance with experimental CO_2 absorption results. In addition, when increasing the absorption temperature from 303.15 K to 323.15 K (the right 4 data points), the misfit, vdW, and total interaction between CO_2 and DES become weaker, indicating that the increment of temperature is not beneficial for the absorption of CO_2 in DES. To sum up, the vdW interaction between CO_2 and DES is the driving force for the CO_2 absorption.

4. Conclusion

The halogen-free and ambient temperature DESs of [3Im:PTSA], [3.5Im:PTSA], and [4Im:PTSA] are selected to dissolve CO_2, and the solubility data is experimentally measured, which confirms the physical absorption behavior of CO_2 in the DESs. The absorption capacity of DESs slightly improves when changing the Im:PTSA mole ratios from 3:1 to 4:1. Increasing temperature or decreasing pressure is conducive to CO_2 absorption. Henry's constant and thermodynamic properties are obtained by correlating with the experimental data. The comparison of molality-based H_m between this work and other reported cases reveals the satisfactory CO_2 absorption capacity of the studied DESs. The small absolute $\Delta_{sol}H$ suggests that it is easier to regenerate, and the positive $\Delta_{sol}G$ reflects that the dissolution of CO_2 is nonspontaneous.

The Jou and Mather empirical model and COSMO-RS model are used to calculate the CO_2 solubility. The former shows an accurate prediction with a small deviation of ARD 5.18 %, taking the experimental data into account. While the latter expresses a good qualitative prediction but a relatively low quantitative result with ARD of 20.80 %, it is acceptable considering the fully predictive character of COSMO-RS. Finally, the interaction energies are calculated by COSMO-RS to analyze the absorption mechanism, which manifests that the vdW interaction between CO_2 and DES is the driving force for the CO_2 absorption. This work demonstrates the promising prospects

of halogen-free DES to capture CO_2.

Declaration of competing interest

The authors declare that they have no known competing financial interests or personal relationships that could have appeared to influence the work reported in this paper.

Acknowledgements

The financial support from National Natural Science Foundation of China (21861132019, 21776074, and 21978096) and Natural Science Foundation of Shanghai (19ZR1412600) is greatly acknowledged. Z. S. gratefully acknowledges the support of the Sino-German joint research project leaded by Deutsche Forschungsgemeinshaft (DFG) under the grants SU 189/9-1.

References

1. G. Siani, M. Tiecco, P. Di Profio, S. Guernelli, A. Fontana, M. Ciulla, V. Canale, Physical absorption of CO_2 in betaine/carboxylic acid-based natural deep eutectic solvents. J. Mol. Liq. 315 (2020) 113708.
2. M.R. Raupach, G. Marland, P. Ciais, C. Le Quere, J.G. Canadell, G. Klepper, C.B. Field, Proc. Natl. Acad. Sci. U. S. A. 104 (2007) 10288-10293.
3. D. Ješić, D.L. Jurković, A. Pohar, L. Suhadolnik, B. Likozar, Engineering photocatalytic and photoelectrocatalytic CO_2 reduction reactions: mechanisms, intrinsic kinetics, mass transfer resistances, reactors and multi-scale modelling simulations. Chem. Eng. J. 2020 126799.
4. J.D. Figueroa, T. Fout, S. Plasynski, H. McIlvried, R.D. Srivastava, Advances in CO_2 capture technology-The U.S. Department of Energy's Carbon Sequestration

Program. Int. J. Greenhouse Gas Control. 2 (2008) 9-20.

5. I.P. Koronaki, L. Prentza, V. Papaefthimiou, Modeling of CO_2 capture via chemical absorption processes - an extensive literature review, Renew. Sust. Energ. Rev. 50 (2015) 547-566.
6. S. Mukherjee, P. Kumar, A. Hosseini, A. Yang, P. Fennell, Comparative assessment of gasification based coal power plants with various CO_2 capture technologies producing electricity and hydrogen. Energ. Fuels 28 (2014) 1028-1040.
7. S. Sarmad, J.P. Mikkola, X.Y. Ji, Carbon dioxide capture with ionic liquids and deep eutectic solvents: a new generation of sorbents. ChemSusChem 10 (2017) 324-352.
8. J. Li, L.F. Chen, Y. Ye, Z.W. Qi, Solubility of CO_2 in the mixed solvent system of alkanolamines and poly (ethylene glycol) 200. J. Chem. Eng. Data 59 (2014) 1781-1787.
9. G.T. Rochelle, Thermal degradation of amines for CO_2 capture, Curr. Opin. Chem. Eng. 1 (2012) 183-190.
10. S.B. Fredriksen, K.-J. Jens, Oxidative degradation of aqueous amine solutions of MEA, AMP, MDEA, Pz: a review, Energ. Procedia 37 (2013) 1770-1777.
11. A. Veawab, P. Tontiwachwuthikul, A. Chakma, Corrosion behavior of carbon steel in the CO_2 absorption process using aqueous amine solutions. Ind. Eng. Chem. Res. 38 (1999) 3917-3924.
12. S. Zeng, X. Zhang, L. Bai, X. Zhang, H. Wang, Ji. Wang, D. Bao, M. Li, X. Liu, S. Zhang, Ionic-liquid-based CO_2 capture systems: structure, interaction and process, Chem. Rev. 117 (2017) 9625-9673.
13. O.B. Ghanem, N. Papaiconomou, M.A. Mutalib, S. Viboud, M. El-Harbawi, Y. Uemura, G. Gonfa, M.A. Bustam, J.M. Lévêque, Thermophysical properties and acute toxicity towards green algae and Vibrio fischeri of amino acid-based ionic liquids. J. Mol. Liq. 212 (2015) 352-359.
14. X.Y. Ji, H. Adidharma, Thermodynamic modeling of CO_2 solubility in ionic liquid with heterosegmented statistical associating fluid theory. Fluid Phase Equilib. 293

(2010) 141-150.

15. X.Y. Ji, H. Adidharma, Thermodynamic modeling of ionic liquid density with heterosegmented statistical associating fluid theory. Chem. Eng. Sci. 64 (2009) 1985-1992.
16. A. S. Amarasekara, Acidic ionic liquids. Chem. Rev. 116 (2016), 6133-6183.
17. Z. Song, T. Zhou, J.N. Zhang, H.Y. Cheng, L.F. Chen, Z.W. Qi, Screening of ionic liquids for solvent-sensitive extraction–with deep desulfurization as an example. Chem. Eng. Sci., 129 (2015), 69-77.
18. M. Kermanioryani, M.I.A. Mutalib, Y. Dong, K.C. Lethesh, O.B. Ghanem, K.A. Kurnia, N.F. Aminuddin, J.M. Leveque. Physicochemical properties of new imidazolium-based ionic liquids containing aromatic group. J. Chem. Eng. Data. 61 (2016) 2020-2026.
19. D. Santos, M. Santos, A. Barison, H. Uslu, D. Datta, S. Mattedi. Protic ionic liquid+ water interactions studied by 1D NOESY NMR spectroscopy. J. Mol. Struct. 1186 (2019) 137-143.
20. D.V. Wagle, H. Zhao, C.A. Deakyne, G.A. Baker. Quantum chemical evaluation of deep eutectic solvents for the extractive desulfurization of fuel. ACS Sustain. Chem. Eng., 6 (2018) 7525-7531.
21. E.L. Smith, A.P. Abbott, K.S Ryder, Deep eutectic solvents (DESs) and their applications. Chem. Rev. 114 (2014), 11060-11082.
22. H. Qin, X.T. Hu, J.W. Wang, H.Y. Cheng, L.F. Chen, Z.W. Qi, Overview of acidic deep eutectic solvents on synthesis, properties and applications. Green Energ. Environ. 5 (2020) 8-21.
23. Q. Zhang, K.D.O. Vigier, S. Royer, F. Jerome, Deep eutectic solvents: syntheses, properties and applications. Chem. Soc. Rev. 41 (2012) 7108-7146.
24. A. Bjelić, B. Hočevar, M. Grilc, U. Novak, B. Likozar, A review of sustainable lignocellulose biorefining applying (natural) deep eutectic solvents (DESs) for separations, catalysis and enzymatic biotransformation processes. Rev. Chem. Eng. (2020) DOI: 10.1515/revce-2019-0077.

25. D.V. Wagle, H. Zhao, G.A. Baker, Deep eutectic solvents: sustainable media for nanoscale and functional materials. Accounts Chem. Res. 47 (2014) 2299-2308.

26. J.L.L. Mamilla, U. Novak, M. Grilc, B. Likozar. Natural deep eutectic solvents (DES) for fractionation of waste lignocellulosic biomass and its cascade conversion to value-added bio-based chemicals. Biomass Bioenergy 120 (2019) 417-425.

27. B. Bojana, U. Novak, B. Likozar. Crustacean shell bio-refining to chitin by natural deep eutectic solvents. Green Process. Synth. 1 (2019) 13-25.

28. A. Diego A., A. Baeza, R. Chinchilla, G. Guillena, I.M. Pastor, D.J. Ramón. Deep eutectic solvents: the organic reaction medium of the century. Eur. J. Org. Chem. 4 (2016) 612-632.

29. A. Tausif, M.S. Nasser, Y. Elhamarnah, M. Magzoub, R. Ullah, H. Qiblawey, S. Aparicio, M. Atilhan. Gas solubility and rheological behavior study of betaine and alanine based natural deep eutectic solvents (NADES). J. Mol. Liq. 256 (2018) 286-295.

30. R.B. Leron, M.H. Li, Solubility of carbon dioxide in a choline chloride-ethylene glycol based deep eutectic solvent. Thermochim. Acta. 551 (2013) 14-19.

31. R.B. Leron, M.H. Li, Solubility of carbon dioxide in a eutectic mixture of choline chloride and glycerol at moderate pressures. J. Chem. Thermodyn. 57 (2013) 131-136.

32. Y.F. Chen, N. Ai, G.H. Li, H.F. Shan, Y.H. Cui, D.S. Deng, Solubilities of carbon dioxide in eutectic mixtures of choline chloride and dihydric alcohols. J. Chem. Eng. Data. 59 (2014) 1247-1253.

33. M.Z. Lu, G.Q. Han, Y.T. Jiang, X.D. Zhang, D.S. Deng, N. Ai, Solubilities of carbon dioxide in the eutectic mixture of levulinic acid (or furfuryl alcohol) and choline chloride. J. Chem. Thermodyn. 88 (2015) 72−77.

34. G.H. Li, D.S. Deng, Y.F. Chen, H.F. Shan, A. Ai, Solubilities and thermodynamic properties of CO2 in choline-chloride based deep eutectic solvents. J. Chem. Thermodyn. 75 (2014), 58-62.

35. J.W. Wang, H.Y. Cheng, Z. Song, L.F. Chen, L. Deng, Z.W. Qi, Carbon dioxide solubility in phosphonium-based deep eutectic solvents: an experimental and molecular dynamics study. Ind. Eng. Chem. Res. 58 (2019) 17514-17523.
36. J. Grasvik, B. Eliasson, J.P. Mikkola. Halogen-free ionic liquids and their utilization as cellulose solvents. J. Mol. Struct. 1028 (2012) 156-163.
37. A. Westerholt, M. Weschta, A. Bosmann, S. Tremmel, Y. Korth, M. Wolf, E. Schlucker, N. Wehrum, A. Lennert, M. Uerdingen, W. Holweger, S. Wartzack, P. Wasserscheid, Halide-free synthesis and tribological performance of oil-miscible ammonium and phosphonium-based ionic liquids. ACS Sustain. Chem. Eng. 3 (2015) 797-808.
38. H. Qin, Z. Song, Q. Zeng, H.Y. Cheng, L.F. Chen, Z.W. Qi, Bifunctional imidazole-PTSA deep eutectic solvent for synthesizing long-chain ester IBIBE in reactive extraction. AIChE J. 65 (2019) 675-683.
39. J. Li, Y. Ye, L. Chen, Z.W. Qi, Solubilities of CO_2 in Poly (ethylene glycols) from (303.15 to 333.15) K. J. Chem. Eng. Data 57 (2012) 610-616.
40. BIPM, IEC, IFCC, ILAC, ISO, IUPAC, IUPAP and OIML, JCGM. 100 (2008) 2008.
41. Q. Zeng, B. Hu, H. Cheng, L. Chen, J. Huang, Z. Qi. Liquid-liquid equilibrium for the system of ionic liquid [BMIm][HSO_4] catalysed isobutyl isobutyrate formation." J. Chem. Thermodynamics 122 (2018) 162-169.
42. J.N. Zhang, L. Qin, D.L. Peng, T. Zhou, H.Y. Cheng, L.F. Chen, Z.W. Qi, COSMO-descriptor based computer-aided ionic liquid design for separation processes: Part II: Task-specific design for extraction processes. Chem. Eng. Sci. 162 (2017) 364-374.
43. Z. Song, T. Zhou, Z.W. Qi, K. Sundmacher. Systematic method for screening ionic liquids as extraction solvents exemplified by an extractive desulfurization process. ACS Sustain. Chem. Eng. 5 (2017) 3382-3389.
44. A.S. Gouveia, F.S. Oliveira, K.A. Kurnia, I.M. Marrucho. Deep eutectic solvents as azeotrope breakers: liquid–liquid extraction and COSMO-RS prediction. ACS Sustain. Chem. Eng. 4 (2016) 5640-5650.

45. Z.G. Lei, C.N. Dai, B.H. Chen. Gas solubility in ionic liquids. Chem. Rev. 114 (2014) 1289-1326.

46. L. Sellaoui, G.L. Dotto, E.C. Peres, Y. Benguerba, É.C. Lima, A.B. Lamine, A. Erto. New insights into the adsorption of crystal violet dye on functionalized multi-walled carbon nanotubes: experiments, statistical physics and COSMO–RS models application. J. Mol. Liq. 248 (2017) 890-897.

47. M. Diedenhofen, A. Klamt, COSMO-RS as a tool for property prediction of IL mixtures-a review. Fluid Phase Equilib. 294 (2010) 31-38.

48. X. Li, X. Liu, D. Deng, Solubilities and thermodynamic properties of CO_2 in four azole-based deep eutectic solvents. J. Chem. Eng. Data 63 (2018) 2091-2096.

49. Z. Song, X.T. Hu, H. Wu, M. Mei, S. Linke, T. Zhou, Z.W. Qi, K. Sundmacher, Systematic screening of deep eutectic solvents as sustainable separation media exemplified by the CO_2 capture process. ACS Sustain. Chem. Eng. 23 (2020) 8741-8751.

50. X. Li, M. Hou, B. Han, X. Wang, L. Zou, Solubility of CO_2 in a choline chloride+ urea eutectic mixture. J. Chem. Eng. Data 53 (2008) 548-550.

51. A. Perez-Salado Kamps, D. Tuma, J. Xia, G. Maurer, Solubility of CO_2 in the ionic liquid [bmim][PF_6]. J. Chem. Eng. Data 48 (2003) 746-749.

52. D.L. Peng, J.N. Zhang, H.Y. Cheng, L.F. Chen, Z.W. Qi, Computer-aided ionic liquid design for separation processes based on group contribution method. Chem. Eng. Sci. 159 (2017) 58-68.

53. N. Aziz, R. Yusoff, M.K. Aroua, Absorption of CO_2 in aqueous mixtures of n-methyldiethanolamine and guanidinium tris(pentafluoroethyl) trifluorophosphate ionic liquid at high-pressure. Fluid Phase Equilib. 322 (2012) 120-125.

54. F.Y. Jou, A.E. Mather, Solubility of carbon dioxide in an aqueous mixture of methyldiethanolamine and n-methylpyrrolidone at elevated pressures. Fluid Phase Equilib. 228 (2005) 465-469.

55. Y.R. Liu, Z.X. Dai, Z.B. Zhang, S.J. Zeng, F.F. Li, X.P. Zhang, Y. Nie, L. Zhang, S.J. Zhang, X.Y. Ji. Ionic liquids/deep eutectic solvents for CO_2 capture: Reviewing

and evaluating. Green Energ. Environ. (2020). https://doi.org/10.1016/j.gee.2020.11.024.

56. X. Liu, B. Gao, Y. Jiang, N. Ai, D. Deng, Solubilities and thermodynamic properties of carbon dioxide in guaiacol-based deep eutectic solvents. J. Chem. Eng. Data 62 (2017) 1448-1455.
57. M. Francisco, A. van den Bruinhorst, L.F. Zubeir, C.J. Peters, M.C. Kroon, A new low transition temperature mixture (LTTM) formed by choline chloride + lactic acid: characterization as solvent for CO_2 capture. Fluid Phase Equilib. 340 (2013) 77-84.
58. Y. Li, W. Huang, D. Zheng, Y. Mi, L. Dong. Solubilities of CO_2 capture absorbents 2-ethoxyethyl ether, 2-butoxyethyl acetate and 2-(2-ethoxyethoxy) ethyl acetate. Fluid Phase Equilibr. 370 (2014) 1-7.
59. D.S. Deng, Y. Chen, Y. Cui, G. Li, N. Ai. Low pressure solubilities of CO_2 in five fatty amine polyoxyethylene ethers. J. Chem. Thermodynamics 72 (2014) 89-93.
60. G. Xia, W. Wang, C. Wang, L. Zhang, Z. Yun, Z. Tang. Vapor-liquid phase equilibrium data of CO_2 in some physical solvents from 285.19 K to 313.26 K. J. Chem. Eng. Data 59 (2014) 844-849.
61. K.A. Kurnia, F. Harris, C.D. Wilfred, M.I. Abdul Mutalib, T. Murugesan, Thermodynamic properties of CO_2 absorption in hydroxyl ammonium ionic liquids at pressures of (100-1600) kPa. J. Chem. Thermodyn. 41 (2009) 1069-1073.
62. M. Costantini, V.A. Toussaint, A. Shariati, C.J. Peters, I. Kikic, High-pressure phase behavior of systems with ionic liquids: part IV. binary system carbon dioxide + 1-hexyl-3-methylimidazolium tetrafluoroborate. J. Chem. Eng. Data 50 (2005) 52-55.